Hot deformation behaviour of low alloyed steel

C. Poletti[1,2,a], S. Großeiber[2,b], S. Ilie[3,c], H.P. Degischer[2,d].

1 IWS. Graz University of Technology. 8010 Graz, Kopernikusgasse 24/I, 8010 Graz, Austria.

2 IMST. Vienna University of Technology, Karlsplatz 13/E308, 1040 Vienna. Austria.

3 Voestalpine Stahl GmbH, Voest-Alpine-Straße 3, Postfach 3, 4031 Linz. Austria

[a]cecilia.poletti@tugraz.at, [b]e0426056@mail.student.tuwien.ac.at, [c]Sergiu.Ilie@voestalpine.com,

[d]peter.degischer@tuwien.ac.at

Keywords: low alloy steel, processing maps, deformation induced ferrite, ductility.

Abstract Hot deformation of a continuously cast low alloyed steel is studied by means of hot compression and tensile tests carried out after austenitization between 700–790 °C at $3x10^{-4}$ – 0.3 s^{-1} of strain rate. The ferrite transformation at the applied cooling rate was determined at 710°C by means of dilatometry. The compressive flow data obtained by using a Gleeble®1500 machine are evaluated to obtain the strain rate sensitivity and the processing maps using different models. The tensile data are used to determine the ductility of the material with different deformation parameters. A new calculation method is used for the instability parameter derived from the dynamic materials model. The strain rate sensitivity does not predict any instability but all the others instability parameters do, including the new one. Pores are formed at the prior austenitic grain boundaries at low strain rates, causing a decay of ductility in the tensile samples. A minimum in the ductility was observed for low strain rates at 750°C. Low strain rates and low temperatures increase the formation of more ferrite than without deformation at the corresponding heat treatments without deformation. In these conditions, the deformation is concentrated in the softer ferrite phase. Low power efficiency was calculated at high strain rates, where no dynamic recrystallization takes place. The domains with similar efficiency of power dissipation are correlated to deformation induced ferrite formation and ferrite recovery. These domains vary with the increasing strain.

Introduction

The hot deformation process parameters (temperature, strain and strain rate) can be correlated with the resulting flow behaviour of metals and their microstructural changes by using different phenomenological and physical methods. The heuristic processing maps developed by Prasad et. al [1] and their modification proposed by Rao and Murty [2] are extensively used for different kinds of materials [3,4]. The processing maps consist of two superimposed maps at constant strain: the efficiency and the instability maps as a function of the temperature and strain rate. A good hot formability of the material should be indicated by high values of dissipation efficiency η and no instabilities. Prasad et al [1] developed the processing maps using the dynamic materials model DMM, were the material is considered essentially dissipative [1]. If the power of dissipation P in the material can be separated into two phenomena [5]: G, thermal transport across the sample and J, microstructural changes [6], then P at a given temperature T and strain ε is expressed as:

$$P_{T,\varepsilon} = \sigma\dot{\varepsilon} = G + J = \int_0^{\dot{\varepsilon}} \sigma d\dot{\varepsilon} + \int_0^{\sigma} \dot{\varepsilon} d\sigma \qquad (1)$$

where σ and $\dot{\varepsilon}$ are the stress and the strain rate, respectively. The efficiency of power dissipation η is defined as a ratio between J and J_{max} = P/2 at T and $\dot{\varepsilon}$. According to DMM and modified DMM, η is defined in the same way, but calculated using different methods. Thus, Rao and Murty proposed to use directly the integrals of Equation 1:

$$\eta = 2\left(P - G\right)/P = 2\left(\sigma\dot{\varepsilon} - \left(\left[\frac{\sigma\dot{\varepsilon}}{m+1} \right]_{\dot{\varepsilon}=\dot{\varepsilon}_{min}} + \int_{\dot{\varepsilon}_{min}}^{\dot{\varepsilon}} \sigma d\dot{\varepsilon} \right) \right) \Big/ \sigma\dot{\varepsilon} \tag{2}$$

with $\dot{\varepsilon}_{min}$ is the minimum strain rate tested and $m = \left[\partial(\ln\sigma)/\partial(\ln\dot{\varepsilon})\right]_{\varepsilon,T}$ the strain rate sensitivity.

The flow instability is related to flow concentrations and represents the restriction by the maximal entropy production during deformation [7], expressed for any function D as [8]:

$$\frac{\partial D}{\partial \dot{\varepsilon}} < \frac{D}{\dot{\varepsilon}} \tag{3}$$

Thus, the flow instability occurs:
1) in the case of D = P (as proposed by Montheillet [9]) when: m < 0
2) in the case of D = J when:

$$\kappa = 2m/\eta - 1 < 0 \tag{4}$$

as proposed by Rao and Murty. [2].
To avoid any correlation with the strain rate sensitivity m, the authors propose to calculate the instability parameter κ as independent form the m value, by using Eq. (5) defining κ_J as in (6):

$$\frac{\partial J}{\partial \dot{\varepsilon}} < \frac{J}{\dot{\varepsilon}} \Rightarrow m\sigma < \frac{J}{\dot{\varepsilon}} \Rightarrow mP < J \tag{5}$$

$$\kappa_J \equiv 1 - \frac{\partial \ln J}{\partial \ln \dot{\varepsilon}} \tag{6}$$

which represents instability of the flow when it is negative.

Finally, the instability parameter α [10] related to the softening was used:

$$\alpha = -\gamma/m \tag{7}$$

The deformation at high temperatures in low alloyed steel takes place generally in the austenite single phase field. The dynamic recovery in austenite is low due to the low stacking fault energy of the fcc phase [11], and at high temperatures tends to dynamically recrystallize (DRX) after reaching a critical strain (ε_C) [12]. In the first part of the flow curve, strain hardening until ε_C takes place before DRX above the critical temperature, or ferrite formation below it occurs, decreasing the flow stress by about 20% [13, 14,15]. The objective of this work is to correlate the flow response of low alloyed steel during hot deformation with the strain rate sensitivity m, efficiency of power dissipation η and instability parameters to interpret the deformation mechanisms near the second minimum of ductility.

Experimental

Material. The micro alloyed steel used in this work contains in wt% 0.194 C, 1.71 Mn, 0.47 Si, 0.11V, 0.022 Cr and 0.022N. The as delivered condition of the material is the continuously cast slab. The samples were taken from near to the surface of the slab, along the casting direction (L). The temperature of austenite to ferrite transformation during cooling at 1K s^{-1} was determined by dilatometry as A_{r3} = 710 °C

Metallography. The samples were cut along the compression axis (L) before and after compression and embedded for metallographic preparation. All the samples for light optical microscopy (LOM) were ground and polished up to 1µm diamond paste and etched with Nital solution and for scanning electron microscopy polished up to 0.04µm SiO_2 colloidal solution. Pictures of deformed samples were taken by means of a field emission gun – scanning electron microscope Quanta 200 FEG.

Hot deformation. Cylindrical compression samples of 15 mm long and 10 mm in diameter, and tensile samples with L_0= 18.5mm and 8mm in diameter were machined. The deformation tests were performed at a constant strain rate using a Gleeble ® 1500 servohydraulic machine. All the samples were heat treated at the austenitization temperature of 1250°C for 1 minute, and then cooled down at 1K s^{-1} to a test temperature between 700-790°C, held there during 30 s and deformed at strain rates of $3x10^{-4}$ s^{-1} (A), $1x10^{-3}$ s^{-1} (B), $3x10^{-3}$ s^{-1} (C), $3x10^{-2}$ s^{-1} (D) and 0.3 s^{-1}(E). Some samples were only heat treated according to the same T(t) exposure and some others deformed at A, C, E and 850 and 950°C. In situ water quenching was applied to freeze the original grain microstructure.

Results

Flow behaviour. The true compression flow curves for strain rates at700, 750 and 790°C are shown in Fig. 1. The curves at strain rates lower than C show softening after a peak stress at 700 and 750°C. At higher strain rates and test temperatures steady state is reached. In Fig. 2 the peak flow stress σ_m in compression (Fig. 2a) as well as tension (Fig.2b) decrease with increasing the temperature for all the tested $\dot{\varepsilon}$.

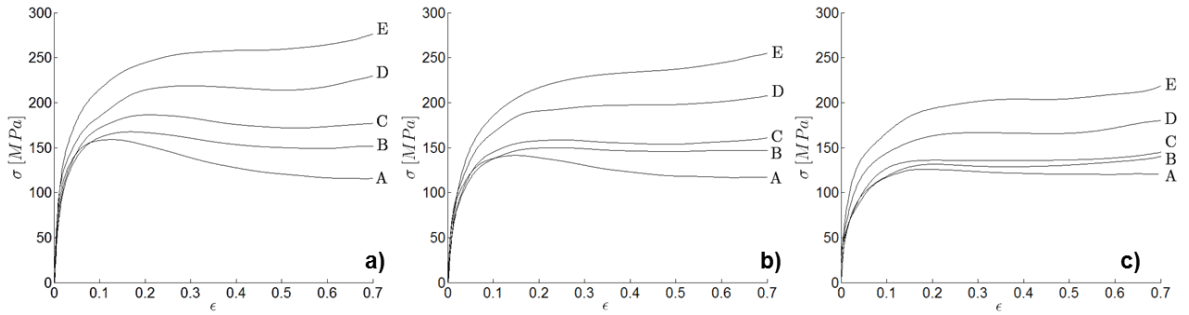

Fig.1 Flow compressive curves at a) 700, b) 750°C and c) 790°C for all the tested strain rates

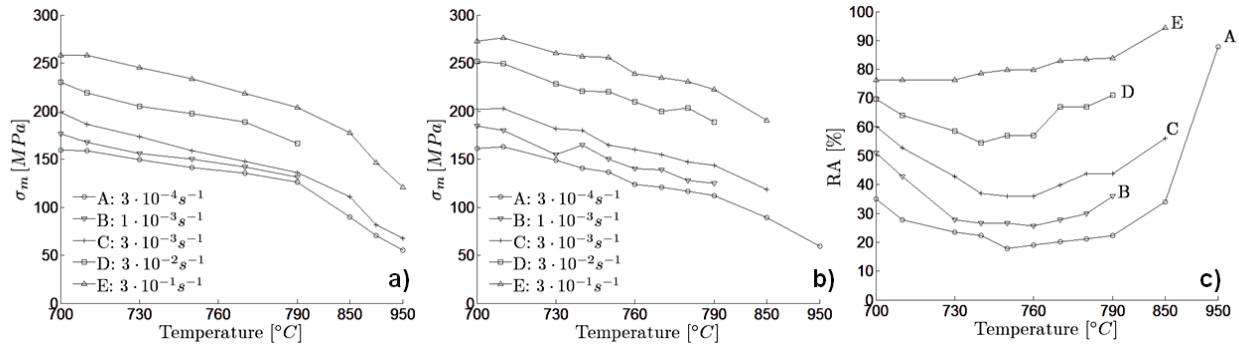

Fig.2 Flow data as a function of the temperature and the strain rate: a) maximal flow compressive stress b) maximal flow tensile stress c) percentage reduction of area after fracture (RA)

The results related to ductility obtained from tensile tests are plotted in Figure 2c, showing that lower strain rates (A) can decrease the reduction in area by a factor of 4 compared with the values at high strain rates (E). The temperature has little influence up to 790°C, and a minimum ductility value is achieved at around 750°C for the lowest strain rate. The RA value increases up to around 85% for all the strain rates when the temperature of deformation is increased up to 950°C.

Processing maps. The instability and the processing maps were generated using Matlab Software. Processing maps deduced from the compressive flow curves are presented in Fig. 3 for different models. The values of flow stress at 0.5 and 0.7 of strain ($\sigma_{0.5}$, and $\sigma_{0.7}$, respectively), were taken from the flow curves at constant temperature and strain rate and used for calculating the m, η, κ, κ_J and α values according to equations presented in the introduction. The isolines represent m or η, and the dashed zones, the instability predicted by κ and κ_J.

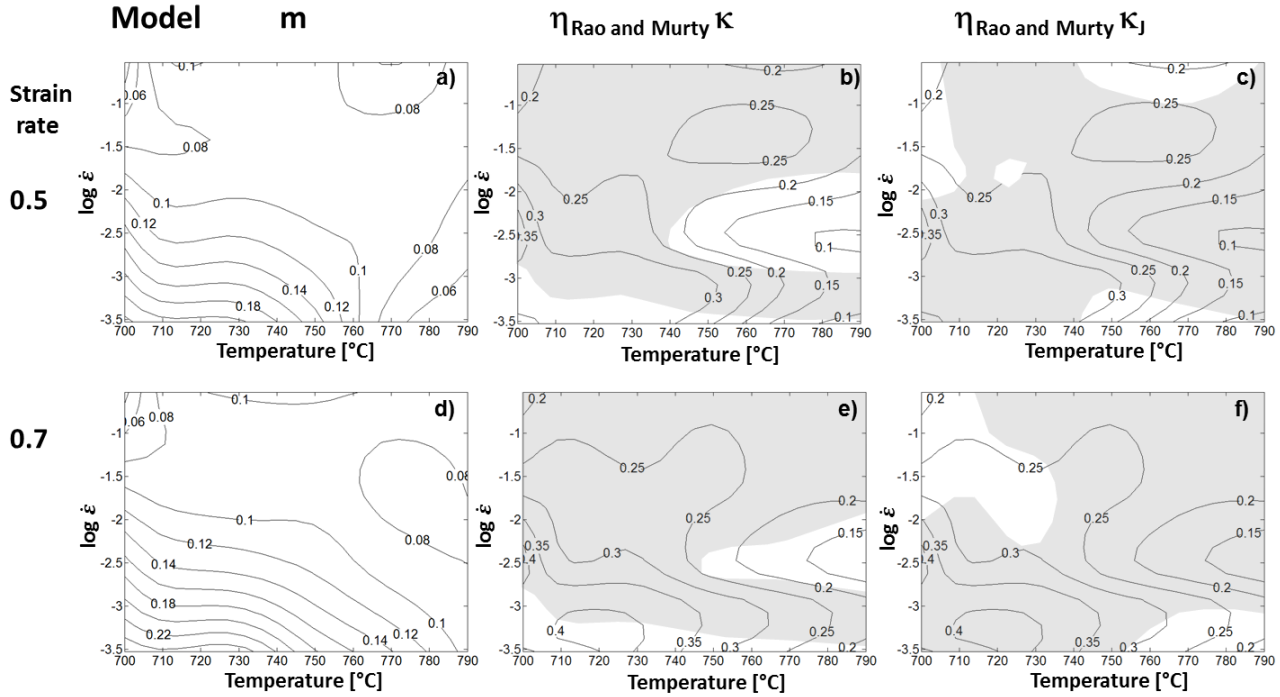

Fig.3 Values as a function of the log strain rate (Y axis) and temperature (X axis) for 0.5 and 0.7 of strain for a,d) m value b,e) efficiency of power dissipation η with κ (dashed) c,f) η with κ_J (dashed)

The m values are positive in the whole tested range. The $\eta_{\text{Rao and Murty}}$ maps follow in general the same tendency as the m ones, with larger values predicted for the low temperature and low strain rate range.

Concerning the stability zones, the different criteria result in diverse instability predictions. As observed in Fig. 3a and d, no m < 0 range was observed, meaning that no instability is predicted by the D = P model. This differs from the pictures shown by the Rao and Murty models, where negative κ values (Fig. 3b,e), and negative κ_J values (Fig. 3c, f) are presented as dashed zones.

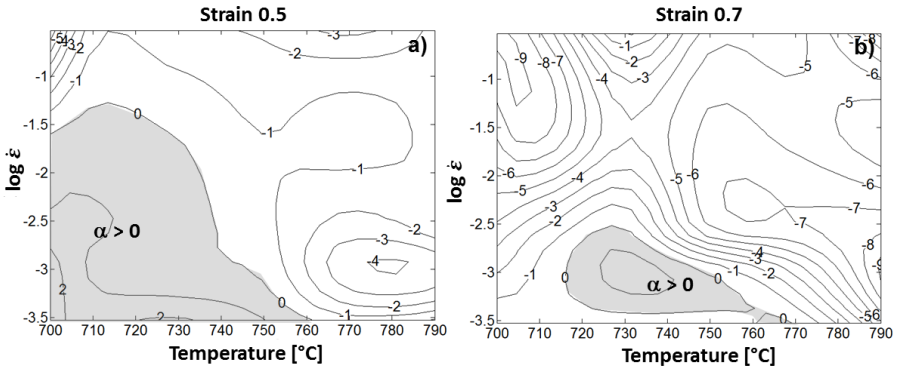

Fig.4 Isolines diagrams of α as a function of the strain rate (Y axis) and the temp. (X axis) for a) 0.5 and b) 0.7 of strain

Finally, it can be observed in Fig.4, that α > 0 (instable flow) in the range of the low strain rates and low temperatures.

Microstructure after hot deformation. Fig 5 shows the developed microstructure of the quenched samples after austenitization and hot compression up to 1 of strain at different parameters. The water quenched samples of all the temperatures and strain rates show a bainitic microstructure transformed from the austenitic phase and some ferrite at the former austenite grain boundaries and along deformation bands. The ferrite films increase with decreasing both temperature and strain

rate. Only the bainitic structure is observed after deformation at 850 and 950 °C for all the strain rates. At low strain rates pores were found at the ferrite - austenite interface. High strain rates provoked a lot of deformation bands, refining the grain structure.

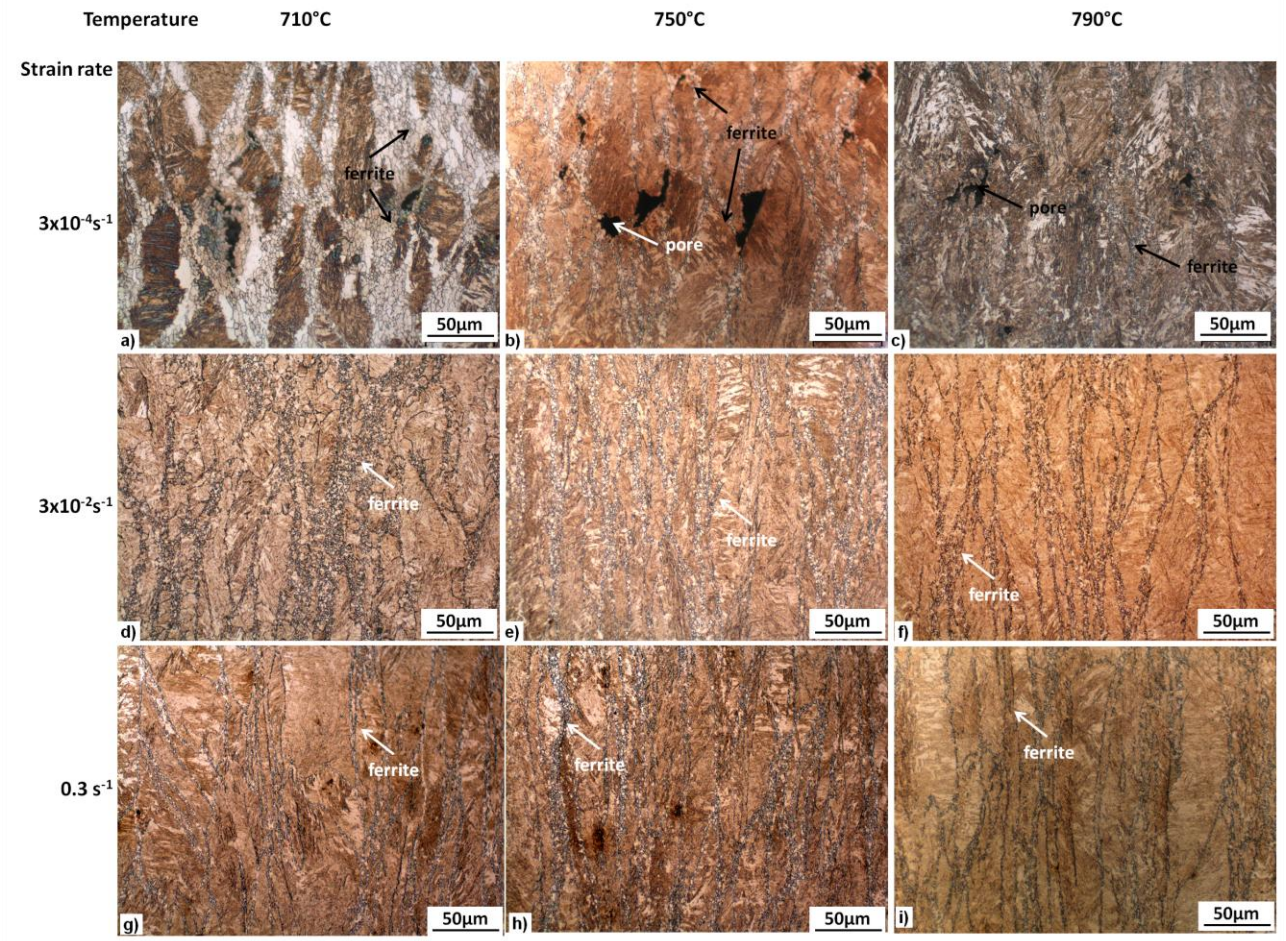

Fig.5 Light optical microscopy of samples water quenched after compression in the horizontal direction. The temperatures and strain rates are included in the graph

FEG-SEM pictures in BSE mode of deformed samples are shown in Fig. 6. The channelling effect allows the differentiation between bainite, ferrite and pores in the samples, corroborating the formation of ferrite even at the strain rate C and 790°C. Fig.6c (710°C and lowest strain rate) shows the formation of VN precipitates.

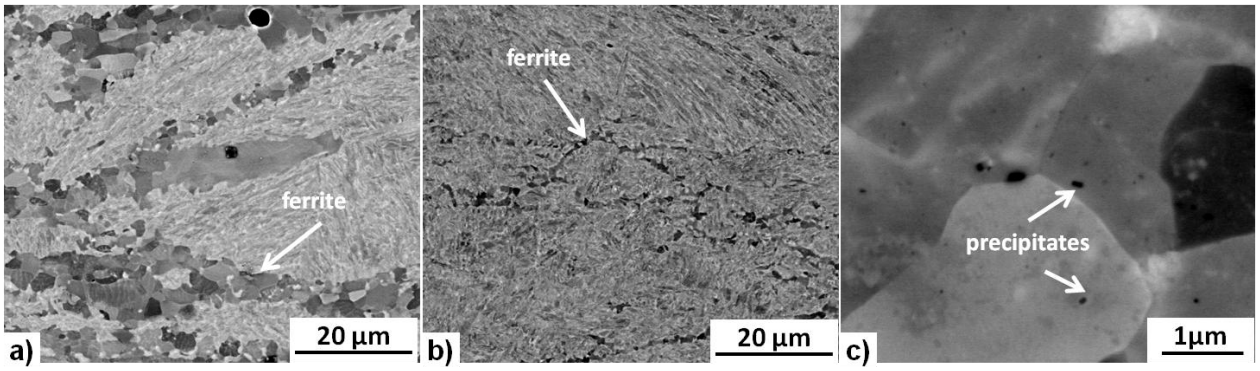

Fig.6 FEG-SEM pictures in BSE mode of samples water quenched after compression in the vertical direction a, b) showing ferrite after deformation at 710°C/A and 790°C/C, respectively, and c) precipitates in a sample deformed at 710°C/A

Discussion and conclusions.

The power dissipation calculated by the modified DMM and the m values can be interpreted by microstructural changes. Instabilities are neither predicted by m in the whole range, nor by κ at low strain rates. On the other hand, the new κ_J predicts instabilities also at low strain rates, and α only at low strain rates, where damage is observed.

The low strain rate area is dominated by the largest η and m values, although they are still smaller than typical values for recrystallization. In this region, softening occurs mainly by ferrite formation [12] at the deformation bands and grain boundaries. Furthermore, the percentage of area reduction is less than the half, porosity is observed at the ferrite/bainite interface and VN rich precipitates form. Both $\alpha > 0$ and $\kappa_J < 0$ criteria predict instabilities which are related to softening due to ferrite formation and damage due to precipitation at the grain boundaries. The first phenomenon results in heterogeneous softening of the material, while the second one is related to strain accumulation at the precipitates, i.e. at grain and subgrain boundaries. Deformation bands and these described phenomena should result in flow instabilities.

At high strain rates deformation bands take place as in the case of low strain rates. This is correlated with low η and m values. In this region, less damage and high ductility of tensile samples occur related to both less ferrite and precipitates formation. The instabilities predicted by κ and κ_J are related to band formation, which are not predicted by α.

Finally, the ductility at low temperatures only increased at temperatures above 850°C, where no ferrite formation was observed, and grain refinement by DRX proceeds.

Acknowledgement

The authors would like to thank to Voestalpine Stahl Linz for the provision of the material and to USTEM (Vienna University of Technology) for the provision of the FEG-SEM EBSD facilities. The project was carried out with Austrian fundings under ZPT via the COMET action for the K-project “Non-destructive Testing and Tomography”.

References

[1]Y.V.R.K Prasad, ,H.L. Gegel, S.M. Doraivelu, J.C. Malas, J.T. Morgan, K.A. Lark, D.R. Barker: Metall. Trans. A15-10 (1984), p. 1883
[2] S.V.S Narayana Murty, B. Nageswara Rao: J. Mater. Sci. Lett. 17 (1998), p. 1203
[3] C. Poletti, H.P. Degischer, S. Kremmer, W. Marketz: Mater. Sci. Eng. A486 (2008), p. 127
[4] S.V.S. Narayana Murty, B. Nageswara Rao: J. Mater. Process. Technol. 104 (2000), p. 103
[5] Y.V.R.K. Prasad: Metall. Mater. Trans. A27 (1996), p. 235.
[6] L. E. Malvern. Introduction to the mechanics of a continuous medium. Prentice-Hall. Series in Engineering of the Physical Sciences. 1969.
[7] S.V.S. Narayana Murty, B. Nageswara Rao, B.P. Kashyap: J. Mater. Proc. Technol. 166 (2) (2005), p. 279
[8] Hans Ziegler. Ed: E. Becker, B. Budiansky, H.A. Lauwerier and T. Koiter. An Introduction to thermomechanics. North-Holland Pulishing Company. 2nd ed. 1983.
[9] F. Montheillet, J.J. Jonas, K.W. Neale: Metall. Mater. Trans. A27 (1996), p. 232
[10] S.L. Semiatin y J.J. Jonas, Formability and Workability of Metals: Plastic Instability and Flow Localization, ASM, Metals Park, Ohio, 1984
[11] F.J. Humphreys and M. Hantherly. Recrystallization and related annealing phenomena (1996)
[12] R. Colás: J. Mater. Process. Technol.62 (1996), p. 180
[13] H.J. McQueen, S. Yue, N.D. Ryan, E. Fry: J. Mater. Process. Tech. 53 (1995), p. 239
[14] J.H. Chung, J.K. Park, T.H. Kim, K.H. Kim, S.Y. Ok: Mater. Sci. Eng. A527 (2010), p. 5072
[15] H. Mirzadeh, A. Najafizadeh: Mater Des 31 (2010), p. 1174